
2 Linear Elastic Fracture Mechanics

The concepts of fracture mechanics that were derived prior to 1960 are applicable only to materials that obey Hooke's law. Although corrections for small-scale plasticity were proposed as early as 1948, these analyses are restricted to structures whose global behavior is linear elastic.

Since 1960, fracture mechanics theories have been developed to account for various types of nonlinear material behavior (i.e., plasticity and viscoplasticity) as well as dynamic effects. All of these more recent results, however, are extensions of linear elastic fracture mechanics (LEFM). Thus a solid background in the fundamentals of LEFM is essential to an understanding of more advanced concepts in fracture mechanics.

This chapter describes both the energy and stress intensity approaches to linear fracture mechanics. The early work of Inglis and Griffith is summarized, followed by an introduction to the energy release rate and stress intensity parameters. The appendix at the end of this chapter includes mathematical derivations of several important results in LEFM.

Subsequent chapters also address linear elastic fracture mechanics. Chapter 7 and Chapter 8 discuss laboratory testing of linear elastic materials, Chapter 9 addresses application of LEFM to structures, Chapter 10 and chapter 11 apply LEFM to fatigue crack propagation and environmental cracking, respectively. Chapter 12 outlines numerical methods for computing stress intensity factor and energy release rate.

2.1 AN ATOMIC VIEW OF FRACTURE

A material fractures when sufficient stress and work are applied at the atomic level to break the bonds that hold atoms together. The bond strength is supplied by the attractive forces between atoms.

Figure 2.1 shows schematic plots of the potential energy and force vs. the separation distance between atoms. The equilibrium spacing occurs where the potential energy is at a minimum. A tensile force is required to increase the separation distance from the equilibrium value; this force must exceed the cohesive force to sever the bond completely. The bond energy is given by

$$E_b = \int_{x_o}^{\infty} P dx \quad (2.1)$$

where x_o is the equilibrium spacing and P is the applied force.

It is possible to estimate the cohesive strength at the atomic level by idealizing the interatomic force-displacement relationship as one half of the period of a sine wave:

$$P = P_c \sin\left(\frac{\pi x}{\lambda}\right) \quad (2.2a)$$

where the distance λ is defined in Figure 2.1. For the sake of simplicity, the origin is defined at x_o . For small displacements, the force-displacement relationship is linear:

$$P = P_c \left(\frac{\pi x}{\lambda} \right) \quad (2.2b)$$

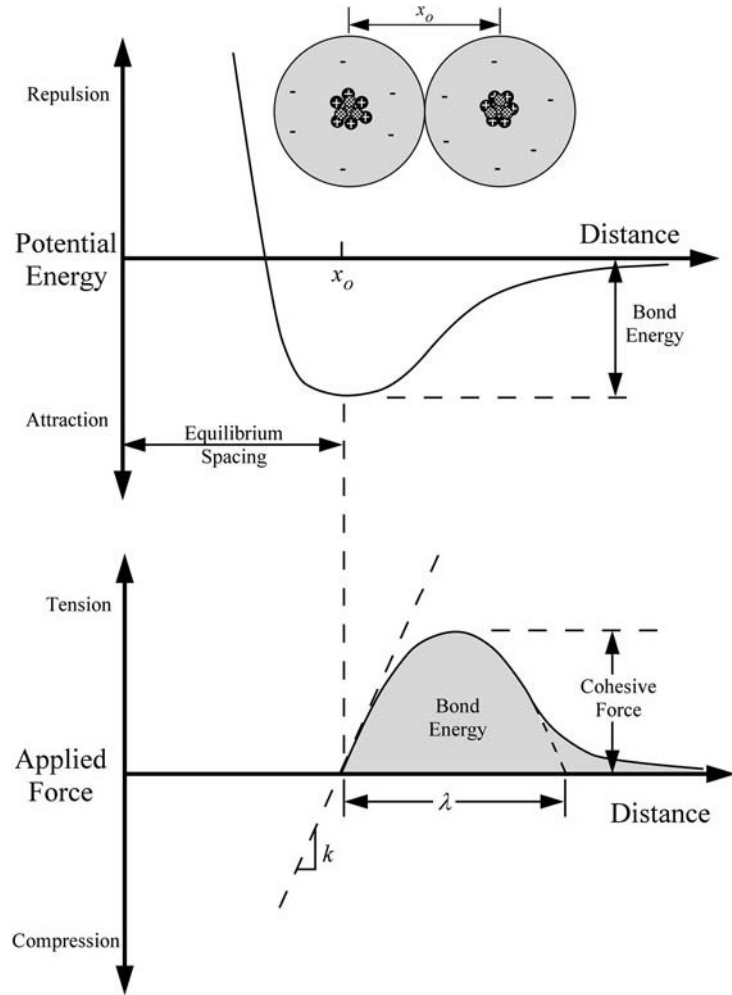


FIGURE 2.1 Potential energy and force as a function of atomic separation. At the equilibrium separation x_o the potential energy is minimized, and the attractive and repelling forces are balanced.

and the bond stiffness (i.e., the spring constant) is given by

$$k = P_c \left(\frac{\pi}{\lambda} \right) \quad (2.3)$$

Multiplying both sides of this equation by the number of bonds per unit area and the gage length, x_o , converts k to Young's modulus E and P_c to the cohesive stress σ_c . Solving for σ_c gives

$$\sigma_c = \frac{E\lambda}{\pi x_o} \quad (2.4)$$

or

$$\sigma_c \approx \frac{E}{\pi} \quad (2.5)$$

if λ is assumed to be approximately equal to the atomic spacing.

The surface energy can be estimated as follows:

$$\gamma_s = \frac{1}{2} \int_0^\lambda \sigma_c \sin\left(\frac{\pi x}{\lambda}\right) dx = \sigma_c \frac{\lambda}{\pi} \quad (2.6)$$

The surface energy per unit area, γ_s , is equal to one-half of the fracture energy because two surfaces are created when a material fractures. Substituting Equation (2.4) into Equation (2.6) and solving for σ_c gives

$$\sigma_c = \sqrt{\frac{E\gamma_s}{x_o}} \quad (2.7)$$

2.2 STRESS CONCENTRATION EFFECT OF FLAWS

The derivation in the previous section showed that the theoretical cohesive strength of a material is approximately E/π , but experimental fracture strengths for brittle materials are typically three or four orders of magnitude below this value. As discussed in Chapter 1, experiments by Leonardo da Vinci, Griffith, and others indicated that the discrepancy between the actual strengths of brittle materials and theoretical estimates was due to flaws in these materials. Fracture cannot occur unless the stress at the atomic level exceeds the cohesive strength of the material. Thus, the flaws must lower the global strength by magnifying the stress locally.

The first quantitative evidence for the stress concentration effect of flaws was provided by Inglis [1], who analyzed elliptical holes in flat plates. His analyses included an elliptical hole $2a$ long by $2b$ wide with an applied stress perpendicular to the major axis of the ellipse (see Figure 2.2). He assumed that the hole was not influenced by the plate boundary, i.e., the plate width $\gg 2a$ and the plate height $\gg 2b$. The stress at the tip of the major axis (Point A) is given by

$$\sigma_A = \sigma \left(1 + \frac{2a}{b}\right) \quad (2.8)$$

The ratio σ_A/σ is defined as the stress concentration factor k_t . When $a = b$, the hole is circular and $k_t = 3.0$, a well-known result that can be found in most strength-of-materials textbooks.

As the major axis, a , increases relative to b , the elliptical hole begins to take on the appearance of a sharp crack. For this case, Inglis found it more convenient to express Equation (2.8) in terms of the radius of curvature ρ :

$$\sigma_A = \sigma \left(1 + 2\sqrt{\frac{a}{\rho}}\right) \quad (2.9)$$

where

$$\rho = \frac{b^2}{a} \quad (2.10)$$

When $a \gg b$, Equation (2.9) becomes

$$\sigma_A = 2\sigma \sqrt{\frac{a}{\rho}} \quad (2.11)$$

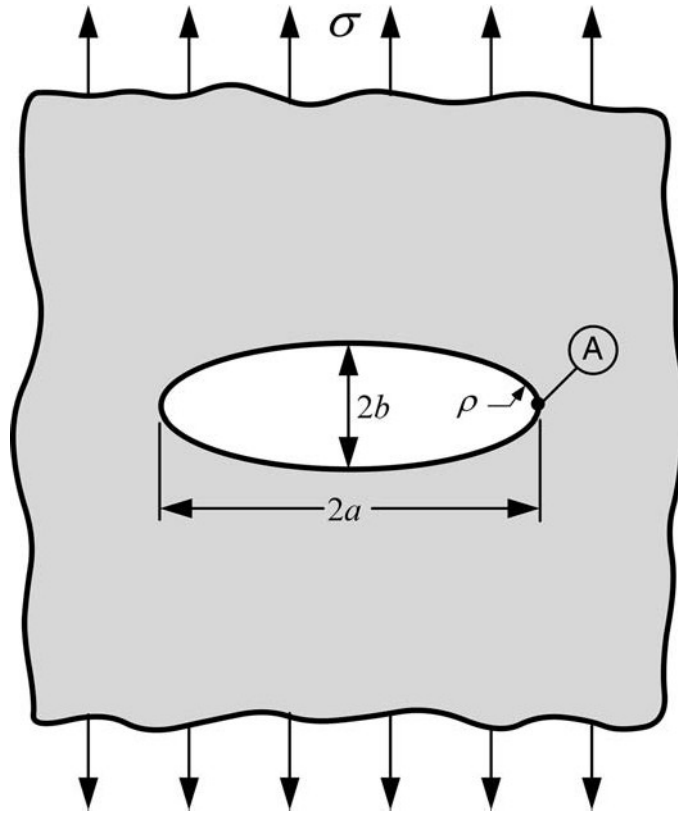


FIGURE 2.2 Elliptical hole in a flat plate.

Inglis showed that Equation (2.11) gives a good approximation for the stress concentration due to a notch that is not elliptical except at the tip.

Equation (2.11) predicts an infinite stress at the tip of an infinitely sharp crack, where $\rho = 0$. This result caused concern when it was first discovered, because no material is capable of withstanding infinite stress. A material that contains a sharp crack should theoretically fail upon the application of an infinitesimal load. The paradox of a sharp crack motivated Griffith [2] to develop a fracture theory based on energy rather than local stress (Section 2.3).

An infinitely sharp crack in a continuum is a mathematical abstraction that is not relevant to real materials, which are made of atoms. Metals, for instance, deform plastically, which causes an initially sharp crack to blunt. In the absence of plastic deformation, the minimum radius a crack tip can have is on the order of the atomic radius. By substituting $\rho = x_o$ into Equation (2.11), we obtain an estimate of the local stress concentration at the tip of an atomically sharp crack:

$$\sigma_A = 2\sigma \sqrt{\frac{a}{x_o}} \quad (2.12)$$

If it is assumed that fracture occurs when $\sigma_A = \sigma_c$, Equation (2.12) can be set equal to Equation (2.7), resulting in the following expression for the remote stress at failure:

$$\sigma_f = \left(\frac{E\gamma_s}{4a} \right)^{1/2} \quad (2.13)$$

Equation (2.13) must be viewed as a rough estimate of failure stress, because the continuum assumption upon which the Inglis analysis is based is not valid at the atomic level. However, Gehlen and Kanninen [3] obtained similar results from a numerical simulation of a crack in a two-dimensional lattice, where discrete “atoms” were connected by nonlinear springs:

$$\sigma_f = \alpha \left(\frac{E\gamma_s}{a} \right)^{1/2} \quad (2.14)$$

where α is a constant, on the order of unity, which depends slightly on the assumed atomic force-displacement law (Equation (2.2)).

2.3 THE GRIFFITH ENERGY BALANCE

According to the first law of thermodynamics, when a system goes from a nonequilibrium state to equilibrium, there is a net decrease in energy. In 1920, Griffith applied this idea to the formation of a crack [2]:

It may be supposed, for the present purpose, that the crack is formed by the sudden annihilation of the tractions acting on its surface. At the instant following this operation, the strains, and therefore the potential energy under consideration, have their original values; but in general, the new state is not one of equilibrium. If it is not a state of equilibrium, then, by the theorem of minimum potential energy, the potential energy is reduced by the attainment of equilibrium; if it is a state of equilibrium, the energy does not change.

A crack can form (or an existing crack can grow) only if such a process causes the total energy to decrease or remain constant. Thus the critical conditions for fracture can be defined as the point where crack growth occurs under equilibrium conditions, with no net change in total energy.

Consider a plate subjected to a constant stress σ which contains a crack $2a$ long (Figure 2.3). Assume that the plate width $\gg 2a$ and that plane stress conditions prevail. (Note that the plates in Figure 2.2 and Figure 2.3 are identical when $a \gg b$). In order for this crack to increase in size, sufficient potential energy must be available in the plate to overcome the surface energy of the material. The Griffith energy balance for an incremental increase in the crack area dA , under equilibrium conditions, can be expressed in the following way:

$$\frac{dE}{dA} = \frac{d\Pi}{dA} + \frac{dW_s}{dA} = 0 \quad (2.15a)$$

or

$$-\frac{d\Pi}{dA} = \frac{dW_s}{dA} \quad (2.15b)$$

where

E = total energy

Π = potential energy supplied by the internal strain energy and external forces

W_s = work required to create new surfaces

For the cracked plate illustrated in Figure 2.3, Griffith used the stress analysis of Inglis [1] to show that

$$\Pi = \Pi_o - \frac{\pi\sigma^2 a^2 B}{E} \quad (2.16)$$

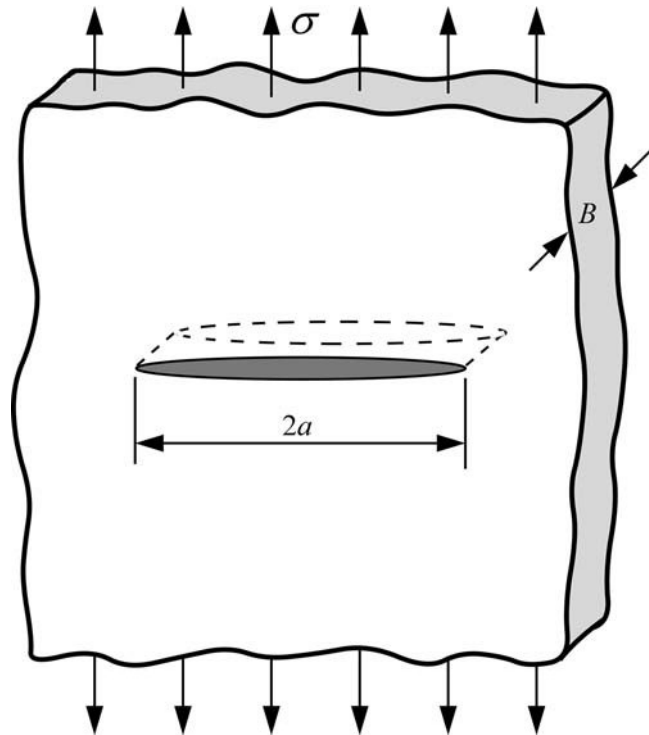


FIGURE 2.3 A through-thickness crack in an infinitely wide plate subjected to a remote tensile stress.

where Π_o is the potential energy of an uncracked plate and B is the plate thickness. Since the formation of a crack requires the creation of two surfaces, W_s is given by

$$W_s = 4aB\gamma_s \quad (2.17)$$

where γ_s is the surface energy of the material. Thus

$$-\frac{d\Pi}{dA} = \frac{\pi\sigma^2 a}{E} \quad (2.18a)$$

and

$$\frac{dW_s}{dA} = 2\gamma_s \quad (2.18b)$$

Equating Equation (2.18a) and Equation (2.18b) and solving for fracture stress gives

$$\sigma_f = \left(\frac{2E\gamma_s}{\pi a} \right)^{1/2} \quad (2.19)$$

It is important to note the distinction between *crack area* and *surface area*. The crack area is defined as the projected area of the crack ($2aB$ in the present example), but since a crack includes two matching surfaces, the surface area is $2A$.

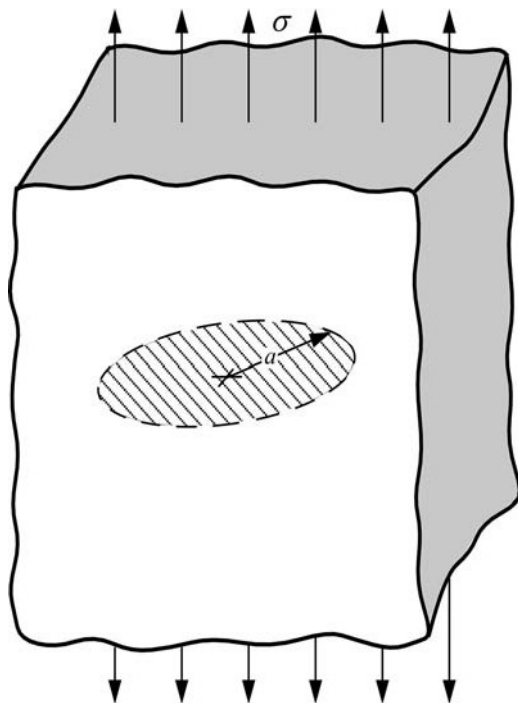


FIGURE 2.4 A penny-shaped (circular) crack embedded in a solid subjected to a remote tensile stress.

The Griffith approach can be applied to other crack shapes. For example, the fracture stress for a penny-shaped flaw embedded in the material (Figure 2.4) is given by

$$\sigma_f = \left(\frac{\pi E \gamma_s}{2(1 - v^2)a} \right)^{1/2} \quad (2.20)$$

where a is the crack radius and v is Poisson's ratio.

2.3.1 COMPARISON WITH THE CRITICAL STRESS CRITERION

The Griffith model is based on a global energy balance: for fracture to occur, the energy stored in the structure must be sufficient to overcome the surface energy of the material. Since fracture involves the breaking of bonds, the stress on the atomic level must be equal to the cohesive stress. This local stress intensification can be provided by flaws in the material, as discussed in Section 2.2.

The similarity between Equation (2.13), Equation (2.14), and Equation (2.19) is obvious. Predictions of the global fracture stress from the Griffith approach and the local stress criterion differ by less than 40%. Thus, these two approaches are consistent with one another, at least in the case of a sharp crack in an ideally brittle solid.

An apparent contradiction emerges when the crack-tip radius is significantly greater than the atomic spacing. The change in the stored energy with crack formation (Equation (2.16)) is insensitive to the notch radius as long as $a \gg b$; thus, the Griffith model implies that the fracture stress is insensitive to ρ . According to the Inglis stress analysis, however, in order for σ_c to be attained at the tip of the notch, σ_f must vary with $1/\sqrt{\rho}$.

Consider a crack with $\rho = 5 \times 10^{-6}$ m. Such a crack would appear sharp under a light microscope, but ρ would be four orders of magnitude larger than the atomic spacing in a typical crystalline solid. Thus the local stress approach would predict a global fracture strength 100 times larger than the Griffith equation. The actual material behavior is somewhere between these extremes; fracture stress does depend on notch root radius, but not to the extent implied by the Inglis stress analysis.

The apparent discrepancy between the critical stress criterion and the energy criterion based on thermodynamics can be resolved by viewing fracture as a nucleation and growth process. When the global stress and crack size satisfy the Griffith energy criterion, there is sufficient thermodynamic driving force to grow the crack, but fracture must first be nucleated. This situation is analogous to the solidification of liquids. Water, for example, is in equilibrium with ice at 0°C, but the liquid-solid reaction requires ice crystals to be nucleated, usually on the surface of another solid (e.g., your car windshield on a January morning). When nucleation is suppressed, liquid water can be super cooled (at least momentarily) to as much as 30°C below the equilibrium freezing point.

Nucleation of fracture can come from a number of sources. For example, microscopic surface roughness at the tip of the flaw could produce sufficient local stress concentration to nucleate failure. Another possibility, illustrated in Figure 2.5, involves a sharp microcrack near the tip of a macroscopic flaw with a finite notch radius. The macroscopic crack magnifies the stress in the vicinity of the microcrack, which propagates when it satisfies the Griffith equation. The microcrack links with the large flaw, which then propagates if the Griffith criterion is satisfied globally. This type of mechanism controls cleavage fracture in ferritic steels, as discussed in Chapter 5.

2.3.2 MODIFIED GRIFFITH EQUATION

Equation (2.19) is valid only for ideally brittle solids. Griffith obtained a good agreement between Equation (2.19) and the experimental fracture strength of glass, but the Griffith equation severely underestimates the fracture strength of metals.

Irwin [4] and Orowan [5] independently modified the Griffith expression to account for materials that are capable of plastic flow. The revised expression is given by

$$\sigma_f = \left(\frac{2E(\gamma_s + \gamma_p)}{\pi a} \right)^{1/2} \quad (2.21)$$

where γ_p is the plastic work per unit area of surface created and is typically much larger than γ_s .

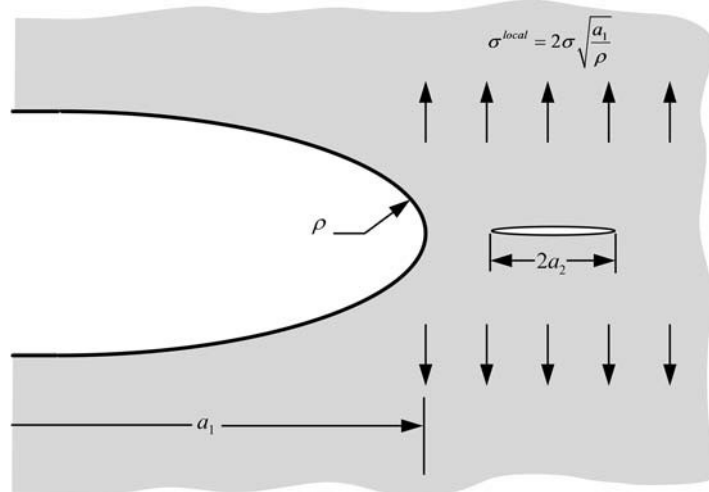


FIGURE 2.5 A sharp microcrack at the tip of a macroscopic crack.

In an ideally brittle solid, a crack can be formed merely by breaking atomic bonds; γ_s reflects the total energy of broken bonds in a unit area. When a crack propagates through a metal, however, a dislocation motion occurs in the vicinity of the crack tip, resulting in additional energy dissipation.

Although Irwin and Orowan originally derived Equation (2.21) for metals, it is possible to generalize the Griffith model to account for any type of energy dissipation:

$$\sigma_f = \left(\frac{2Ew_f}{\pi a} \right)^{1/2} \quad (2.22)$$

where w_f is the fracture energy, which could include plastic, viscoelastic, or viscoplastic effects, depending on the material. The fracture energy can also be influenced by crack meandering and branching, which increase the surface area. Figure 2.6 illustrates various types of material behavior and the corresponding fracture energy.

A word of caution is necessary when applying Equation (2.22) to materials that exhibit nonlinear deformation. The Griffith model, in particular Equation (2.16), applies only to linear elastic material behavior. Thus, the global behavior of the structure must be elastic. Any nonlinear effects, such as plasticity, must be confined to a small region near the crack tip. In addition, Equation (2.22) assumes that w_f is constant; in many ductile materials, the fracture energy increases with crack growth, as discussed in Section 2.5.

EXAMPLE 2.1

A flat plate made from a brittle material contains a macroscopic through-thickness crack with half length a_1 and notch tip radius ρ . A sharp penny-shaped microcrack with radius a_2 is located near the tip of the larger flaw, as illustrated in Figure 2.5. Estimate the minimum size of the microcrack required to cause failure in the plate when the Griffith equation is satisfied by the global stress and a_1 .

Solution: The nominal stress at failure is obtained by substituting a_1 into Equation (2.19). The stress in the vicinity of the microcrack can be estimated from Equation (2.11), which is set equal to the Griffith criterion for the penny-shaped microcrack (Equation 2.20):

$$2 \left(\frac{2E\gamma_s}{\pi a_1} \right)^{1/2} \sqrt{\frac{a_1}{\rho}} = \left(\frac{\pi E\gamma_s}{2(1-v^2)a_2} \right)^{1/2}$$

Solving for a_2 gives

$$a_2 = \frac{\pi^2 \rho}{16(1-v^2)}$$

for $v = 0.3$, $a_2 = 0.68\rho$. Thus the nucleating microcrack must be approximately the size of the macroscopic crack-tip radius.

This derivation contains a number of simplifying assumptions. The notch-tip stress computed from Equation (2.11) is assumed to act uniformly ahead of the notch, in the region of the microcrack; the actual stress would decay away from the notch tip. Also, this derivation neglects free boundary effects from the tip of the macroscopic notch.

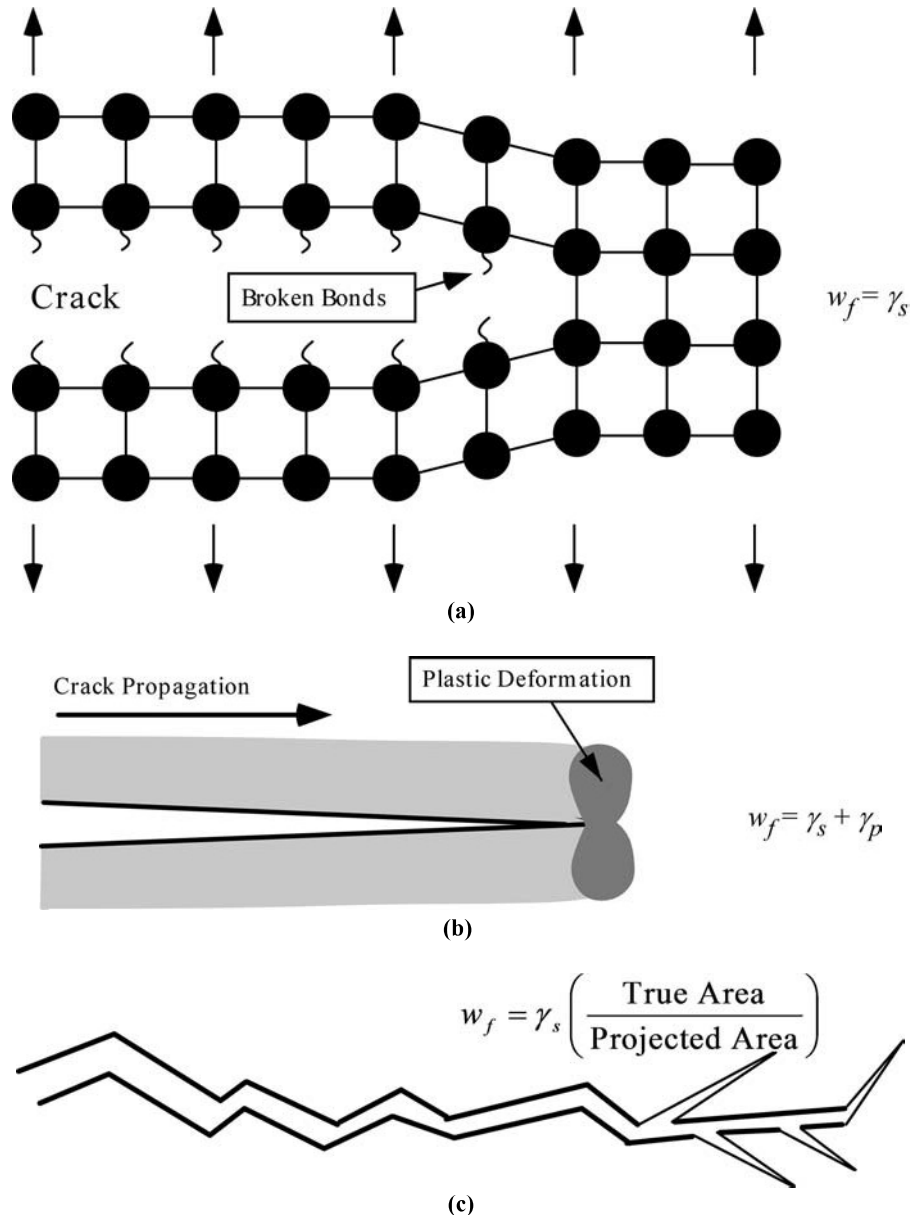


FIGURE 2.6 Crack propagation in various types of materials, with the corresponding fracture energy. (a) ideally brittle material, (b) quasi-brittle elastic-plastic material and, (c) brittle material with crack meandering and branching.

2.4 THE ENERGY RELEASE RATE

In 1956, Irwin [6] proposed an energy approach for fracture that is essentially equivalent to the Griffith model, except that Irwin's approach is in a form that is more convenient for solving engineering problems. Irwin defined an *energy release rate* G , which is a measure of the energy available for an increment of crack extension:

$$G = -\frac{d\Pi}{dA} \quad (2.23)$$

The term *rate*, as it is used in this context, does not refer to a derivative with respect to time; G is the rate of change in potential energy with the crack area. Since G is obtained from the derivative of a potential, it is also called the *crack extension force* or the *crack driving force*. According to Equation (2.18a), the energy release rate for a wide plate in plane stress with a crack of length $2a$ (Figure 2.3) is given by

$$G = \frac{\pi \sigma^2 a}{E} \quad (2.24)$$

Referring to the previous section, crack extension occurs when G reaches a critical value, i.e.,

$$G_c = \frac{dW_s}{dA} = 2w_f \quad (2.25)$$

where G_c is a measure of the *fracture toughness* of the material.

The potential energy of an elastic body, Π , is defined as follows:

$$\Pi = U - F \quad (2.26)$$

where U is the strain energy stored in the body and F is the work done by external forces.

Consider a cracked plate that is dead loaded, as illustrated in Figure 2.7. Since the load is fixed at P , the structure is said to be *load controlled*. For this case

$$F = P\Delta$$

and

$$U = \int_0^\Delta P d\Delta = \frac{P\Delta}{2}$$

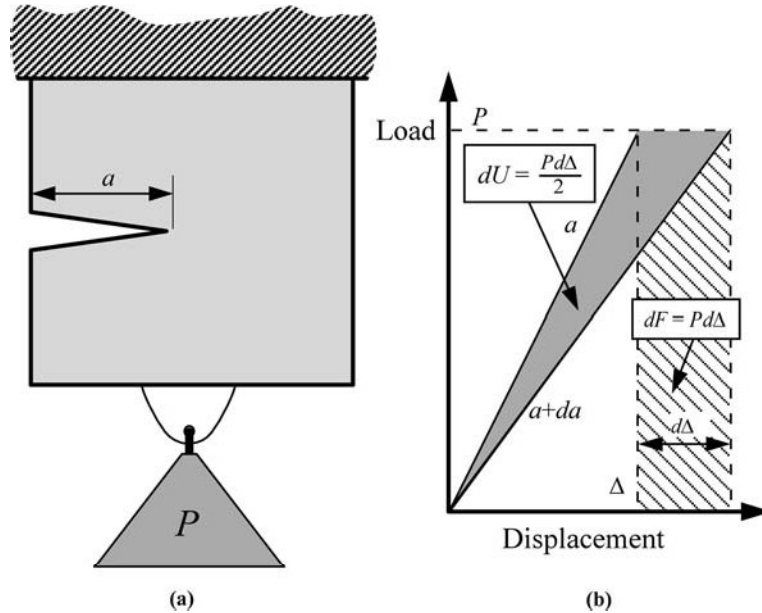


FIGURE 2.7 Cracked plate at a fixed load P .

Therefore

$$\Pi = -U$$

and

$$G = \frac{1}{B} \left(\frac{dU}{da} \right)_p = \frac{P}{2B} \left(\frac{d\Delta}{da} \right)_p \quad (2.27)$$

When displacement is fixed (Figure 2.8), the plate is *displacement controlled*; $F = 0$ and $\Pi = U$. Thus

$$G = -\frac{1}{B} \left(\frac{dU}{da} \right)_\Delta = -\frac{\Delta}{2B} \left(\frac{dP}{da} \right)_\Delta \quad (2.28)$$

It is convenient at this point to introduce the compliance, which is the inverse of the plate stiffness:

$$C = \frac{\Delta}{P} \quad (2.29)$$

By substituting Equation (2.29) into Equation (2.27) and Equation (2.28) it can be shown that

$$G = \frac{P^2}{2B} \frac{dC}{da} \quad (2.30)$$

for both load control and displacement control. Therefore, the energy release rate, as defined in Equation (2.23), is the same for load control and displacement control. Also

$$\left(\frac{dU}{da} \right)_p = -\left(\frac{dU}{da} \right)_\Delta \quad (2.31)$$

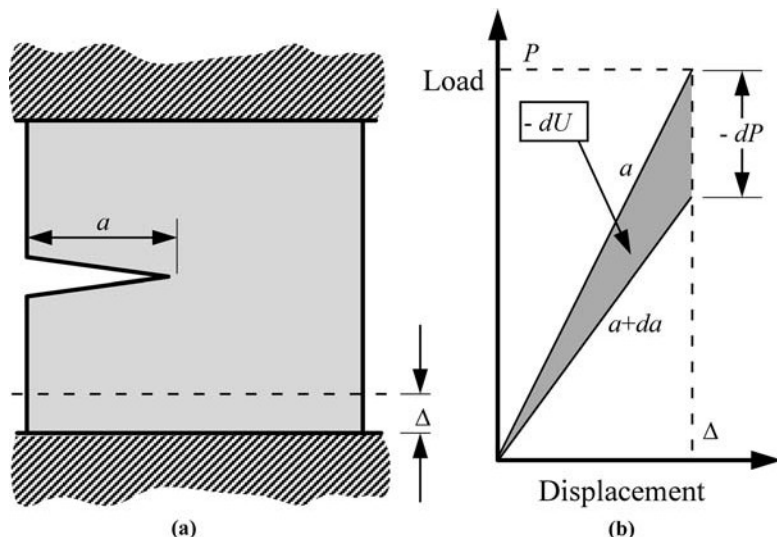


FIGURE 2.8 Cracked plate at a fixed displacement Δ .

Equation (2.31) is demonstrated graphically in Figure 2.7(b) and Figure 2.8(b). In load control, a crack extension da results in a net *increase* in strain energy because of the contribution of the external force P :

$$(dU)_P = Pd\Delta - \frac{Pd\Delta}{2} = \frac{Pd\Delta}{2}$$

When displacement is fixed, $dF = 0$ and the strain energy *decreases*:

$$(dU)_\Delta = \frac{\Delta dP}{2}$$

where dP is negative. As can be seen in Figure 2.7(b) and Figure 2.8(b), the absolute values of these energies differ by the amount $dPd\Delta/2$, which is negligible. Thus

$$(dU)_P = -(dU)_\Delta$$

for an increment of crack growth at a given P and Δ .

EXAMPLE 2.2

Determine the energy release rate for a double cantilever beam (DCB) specimen (Figure 2.9)

Solution: From beam theory

$$\frac{\Delta}{2} = \frac{Pa^3}{3EI} \quad \text{where} \quad I = \frac{Bh^3}{12}$$

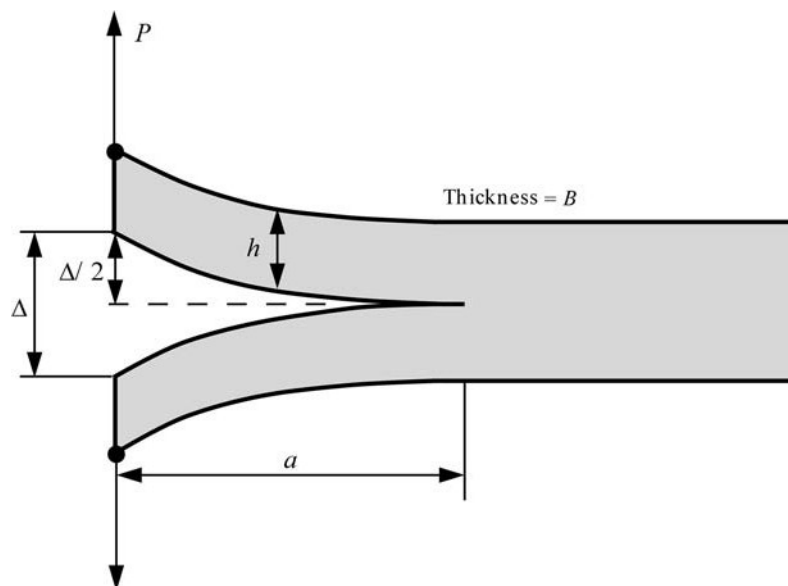


FIGURE 2.9 Double cantilever beam (DCB) specimen.

The elastic compliance is given by

$$C = \frac{\Delta}{P} = \frac{2a^3}{3EI}$$

Substituting C into Equation (2.30) gives

$$G = \frac{P^2 a^2}{BEI} = \frac{12 P^2 a^2}{B^2 h^3 E}$$

2.5 INSTABILITY AND THE R CURVE

Crack extension occurs when $G = 2w_f$; but crack growth may be stable or unstable, depending on how G and w_f vary with crack size. To illustrate stable and unstable behavior, it is convenient to replace $2w_f$ with R , the material resistance to crack extension. A plot of R vs. crack extension is called a *resistance curve* or *R curve*. The corresponding plot of G vs. crack extension is the *driving force curve*.

Consider a wide plate with a through crack of initial length $2a_0$ (Figure 2.3). At a fixed remote stress σ , the energy release rate varies linearly with crack size (Equation (2.24)). Figure 2.10 shows schematic driving force vs. R curves for two types of material behavior.

The first case, Figure 2.10(a), shows a flat R curve, where the material resistance is constant with crack growth. When the stress is σ_1 , the crack is stable. Fracture occurs when the stress reaches σ_2 ; the crack propagation is unstable because the driving force increases with crack growth, but the material resistance remains constant.

Figure 2.10(b) illustrates a material with a rising R curve. The crack grows a small amount when the stress reaches σ_2 , but cannot grow further unless the stress increases. When the stress is fixed at σ_2 , the driving force increases at a slower rate than R . Stable crack growth continues as the stress increases to σ_3 . Finally, when the stress reaches σ_4 , the driving force curve is tangent to the R curve. The plate is unstable with further crack growth because the rate of change in the driving force exceeds the slope of the R curve.

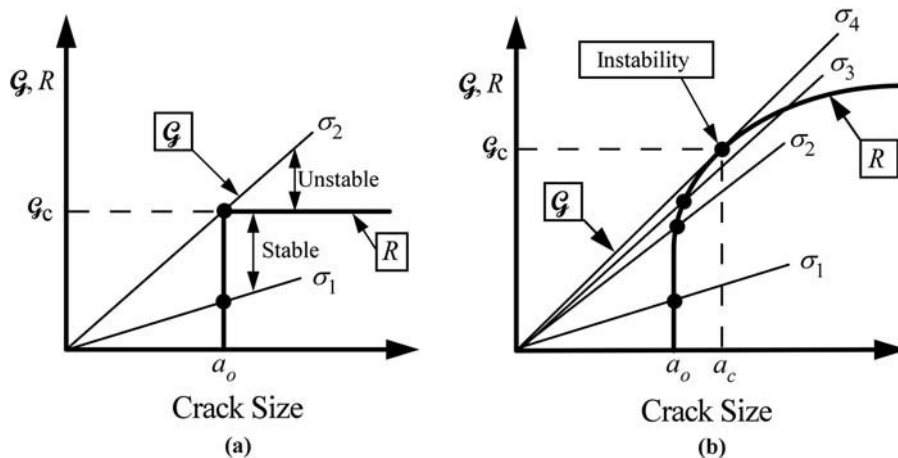


FIGURE 2.10 Schematic driving force vs. R curve diagrams (a) flat R curve and (b) rising R curve.

The conditions for *stable* crack growth can be expressed as follows:

$$\mathcal{G} = R \quad (2.32a)$$

and

$$\frac{d\mathcal{G}}{da} \leq \frac{dR}{da} \quad (2.32b)$$

Unstable crack growth occurs when

$$\frac{d\mathcal{G}}{da} > \frac{dR}{da} \quad (2.33)$$

When the resistance curve is flat, as in Figure 2.10(a), one can define a critical value of energy release rate \mathcal{G}_c , unambiguously. A material with a rising R curve, however, cannot be uniquely characterized with a single toughness value. According to Equation (2.33) a flawed structure fails when the driving force curve is tangent to the R curve, but this point of tangency depends on the shape of the driving force curve, which depends on the configuration of the structure. The driving force curve for the through crack configuration is linear, but \mathcal{G} in the DCB specimen (Example 2.2) varies with a^2 ; these two configurations would have different \mathcal{G}_c values for a given R curve.

Materials with rising R curves can be characterized by the value of \mathcal{G} at the initiation of the crack growth. Although the initiation toughness is usually not sensitive to structural geometry, there are other problems with this measurement. It is virtually impossible to determine the precise moment of crack initiation in most materials. An engineering definition of initiation, analogous to the 0.2% offset yield strength in tensile tests, is usually required. Another limitation of initiation toughness is that it characterizes only the onset of crack growth; it provides no information on the shape of the R curve.

2.5.1 REASONS FOR THE R CURVE SHAPE

Some materials exhibit a rising R curve, while the R curve for other materials is flat. The shape of the R curve depends on the material behavior and, to a lesser extent, on the configuration of the cracked structure.

The R curve for an ideally brittle material is flat because the surface energy is an invariant material property. When nonlinear material behavior accompanies fracture, however, the R curve can take on a variety of shapes. For example, ductile fracture in metals usually results in a rising R curve; a plastic zone at the tip of the crack increases in size as the crack grows. The driving force must increase in such materials to maintain the crack growth. If the cracked body is infinite (i.e., if the plastic zone is small compared to the relevant dimensions of the body) the plastic zone size and R eventually reach steady-state values, and the R curve becomes flat with further growth (see Section 3.5.2).

Some materials can display a falling R curve. When a metal fails by cleavage, for example, the material resistance is provided by the surface energy and local plastic dissipation, as illustrated in Figure 2.6(b). The R curve would be relatively flat if the crack growth were stable. However, cleavage propagation is normally unstable; the material near the tip of the growing crack is subject to very high strain rates, which suppress plastic deformation. Thus, the resistance of a rapidly growing cleavage crack is less than the initial resistance at the onset of fracture.

The size and geometry of the cracked structure can exert some influence on the shape of the R curve. A crack in a thin sheet tends to produce a steeper R curve than a crack in a thick plate because there is a low degree of stress triaxiality at the crack tip in the thin sheet, while the material near the tip of the crack in the thick plate may be in plane strain. The R curve can also be affected if the growing crack approaches a free boundary in the structure. Thus, a wide plate may exhibit a somewhat different crack growth resistance behavior than a narrow plate of the same material.

Ideally, the R curve, as well as other measures of fracture toughness, should be a property only of the material and not depend on the size or shape of the cracked body. Much of fracture mechanics is predicated on the assumption that fracture toughness is a material property. Configurational effects can occur, however. A practitioner of fracture mechanics should be aware of these effects and their potential influence on the accuracy of an analysis. This issue is explored in detail in Section 2.10, Section 3.5, and Section 3.6.

2.5.2 LOAD CONTROL VS. DISPLACEMENT CONTROL

According to Equation (2.32) and Equation (2.33), the stability of crack growth depends on the rate of change in G , i.e., the second derivative of potential energy. Although the driving force G is the same for both load control and displacement control, the *rate of change* of the driving force curve depends on how the structure is loaded.

Displacement control tends to be more stable than load control. With some configurations, the driving force actually decreases with crack growth in displacement control. A typical example is illustrated in Figure 2.11.

Referring to Figure 2.11, consider a cracked structure subjected to a load P_3 and a displacement Δ_3 . If the structure is load controlled, it is at the point of instability where the driving force curve is tangent to the R curve. In displacement control, however, the structure is stable because the driving force decreases with crack growth; the displacement must be increased for further crack growth.

When an R curve is determined experimentally, the specimen is usually tested in displacement control, or as near to pure displacement control as is possible in the test machine. Since most of the common test specimen geometries exhibit falling driving force curves in displacement control,

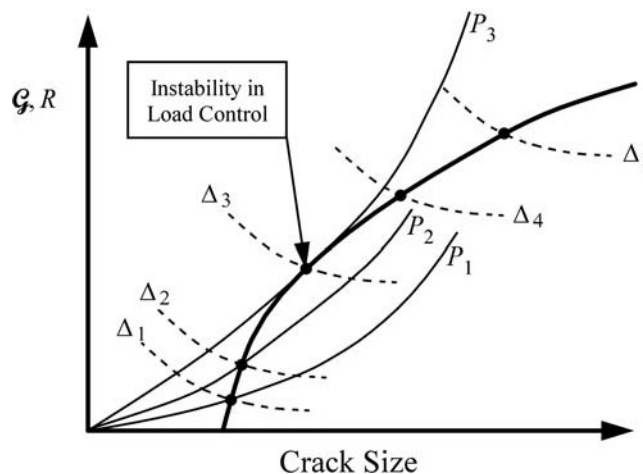


FIGURE 2.11 Schematic driving force/ R curve diagram that compares load control and displacement control.

it is possible to obtain a significant amount of stable crack growth. If an instability occurs during the test, the R curve cannot be defined beyond the point of ultimate failure.

EXAMPLE 2.3

Evaluate the relative stability of a DCB specimen (Figure 2.9) in load control and displacement control.

Solution: From the result derived in Example 2.2, the slope of the driving force curve in load control is given by

$$\left(\frac{d\mathcal{G}}{da} \right)_P = \frac{2P^2a}{BEI} = \frac{2\mathcal{G}}{a}$$

In order to evaluate displacement control, it is necessary to express \mathcal{G} in terms of Δ and a . From beam theory, load is related to displacement as follows:

$$P = \frac{3\Delta EI}{2a^3}$$

Substituting the above equation into expression for energy release rate gives

$$\mathcal{G} = \frac{9\Delta^2 EI}{4Ba^4}$$

Thus

$$\left(\frac{d\mathcal{G}}{da} \right)_\Delta = -\frac{9\Delta^2 EI}{Ba^5} = -\frac{4\mathcal{G}}{a}$$

Therefore, the driving force increases with crack growth in load control and decreases in displacement control. For a flat R curve, crack growth in load control is always unstable, while displacement control is always stable.

2.5.3 STRUCTURES WITH FINITE COMPLIANCE

Most real structures are subject to conditions between load control and pure displacement control. This intermediate situation can be schematically represented by a spring in series with the flawed structure (Figure 2.12). The structure is fixed at a constant remote displacement Δ_T ; the spring represents the system compliance C_m . Pure displacement control corresponds to an infinitely stiff spring, where $C_m = 0$. Load control (dead loading) implies an infinitely soft spring, i.e., $C_m = \infty$.

When the system compliance is finite, the point of fracture instability obviously lies somewhere between the extremes of pure load control and pure displacement control. However, determining the precise point of instability requires a rather complex analysis.

At the moment of instability, the following conditions are satisfied:

$$\mathcal{G} = R \quad (2.34a)$$

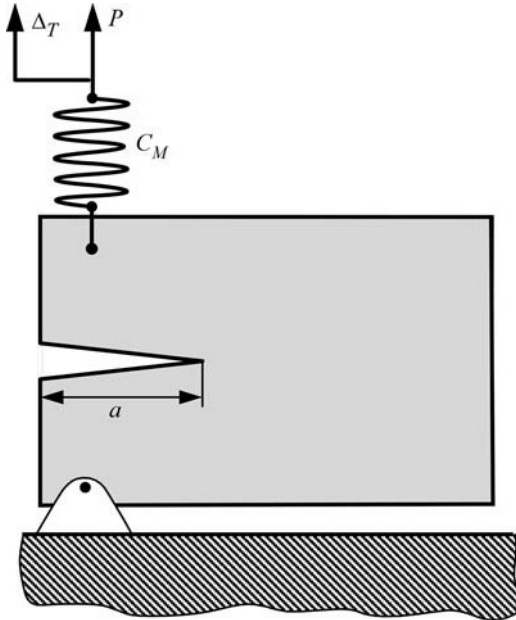


FIGURE 2.12 A cracked structure with finite compliance, represented schematically by a spring in series.

and

$$\left(\frac{d\mathcal{G}}{da} \right)_{\Delta_T} = \frac{dR}{da} \quad (2.34b)$$

The left side of Equation (2.34b) is given by Hutchinson and Paris [7]

$$\left(\frac{d\mathcal{G}}{da} \right)_{\Delta_T} = \left(\frac{\partial \mathcal{G}}{\partial a} \right)_P - \left(\frac{\partial \mathcal{G}}{\partial P} \right)_a \left(\frac{\partial \Delta}{\partial a} \right)_P \left[C_m + \left(\frac{\partial \Delta}{\partial P} \right)_a \right]^{-1} \quad (2.35)$$

Equation (2.35) is derived in Appendix 2.2.

2.6 STRESS ANALYSIS OF CRACKS

For certain cracked configurations subjected to external forces, it is possible to derive closed-form expressions for the stresses in the body, assuming isotropic linear elastic material behavior. Westergaard [8], Irwin [9], Sneddon [10], and Williams [11] were among the first to publish such solutions. If we define a polar coordinate axis with the origin at the crack tip (Figure 2.13), it can be shown that the stress field in any linear elastic cracked body is given by

$$\sigma_{ij} = \left(\frac{k}{\sqrt{r}} \right) f_{ij}(\theta) + \sum_{m=0}^{\infty} A_m r^{\frac{m}{2}} g_{ij}^{(m)}(\theta) \quad (2.36)$$

where

σ_{ij} = stress tensor

r and θ are as defined in Figure 2.13

k = constant

f_{ij} = dimensionless function of θ in the leading term

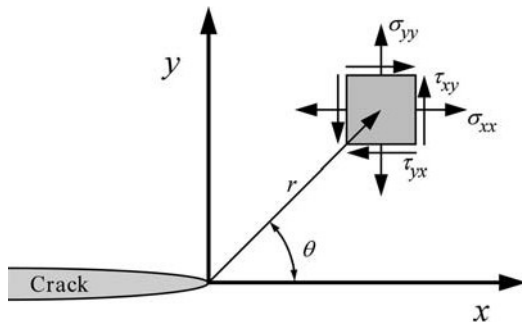


FIGURE 2.13 Definition of the coordinate axis ahead of a crack tip. The z direction is normal to the page.

For the higher-order terms, A_m is the amplitude and $g_{ij}^{(m)}$ is a dimensionless function of θ for the m th term. The higher-order terms depend on geometry, but the solution for any given configuration contains a leading term that is proportional to $1/\sqrt{r}$. As $r \rightarrow 0$, the leading term approaches infinity, but the other terms remain finite or approach zero. Thus, stress near the crack tip varies with $1/\sqrt{r}$, regardless of the configuration of the cracked body. It can also be shown that displacement near the crack tip varies with \sqrt{r} . Equation (2.36) describes a stress *singularity*, since stress is asymptotic to $r = 0$. The basis of this relationship is explored in more detail in Appendix 2.3.

There are three types of loading that a crack can experience, as Figure 2.14 illustrates. Mode I loading, where the principal load is applied normal to the crack plane, tends to open the crack. Mode II corresponds to in-plane shear loading and tends to slide one crack face with respect to the other. Mode III refers to out-of-plane shear. A cracked body can be loaded in any one of these modes, or a combination of two or three modes.

2.6.1 THE STRESS INTENSITY FACTOR

Each mode of loading produces the $1/\sqrt{r}$ singularity at the crack tip, but the proportionality constants k and f_{ij} depend on the mode. It is convenient at this point to replace k by the *stress intensity factor* K , where $K = k\sqrt{2\pi}$. The stress intensity factor is usually given a subscript to denote the mode of loading, i.e., K_I , K_{II} , or K_{III} . Thus, the stress fields ahead of a crack tip in an isotropic linear elastic

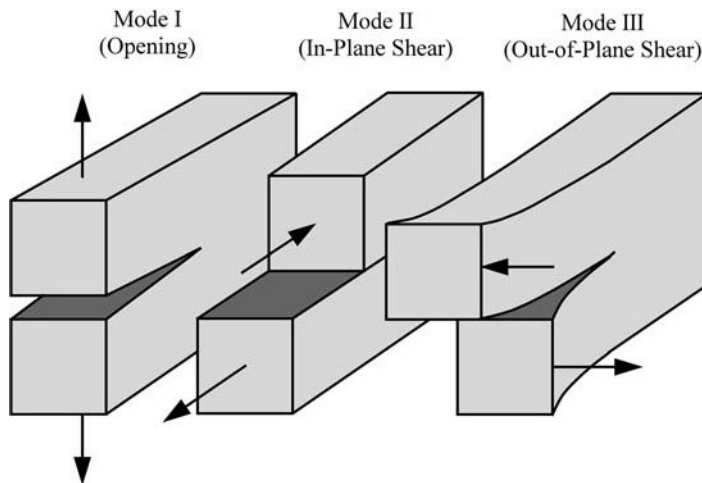


FIGURE 2.14 The three modes of loading that can be applied to a crack.

TABLE 2.1
Stress Fields Ahead of a Crack Tip for Mode I and Mode II
in a Linear Elastic, Isotropic Material

	Mode I	Mode II
σ_{xx}	$\frac{K_I}{\sqrt{2\pi r}} \cos\left(\frac{\theta}{2}\right) \left[1 - \sin\left(\frac{\theta}{2}\right) \sin\left(\frac{3\theta}{2}\right) \right]$	$-\frac{K_{II}}{\sqrt{2\pi r}} \sin\left(\frac{\theta}{2}\right) \left[2 + \cos\left(\frac{\theta}{2}\right) \cos\left(\frac{3\theta}{2}\right) \right]$
σ_{yy}	$\frac{K_I}{\sqrt{2\pi r}} \cos\left(\frac{\theta}{2}\right) \left[1 + \sin\left(\frac{\theta}{2}\right) \sin\left(\frac{3\theta}{2}\right) \right]$	$\frac{K_{II}}{\sqrt{2\pi r}} \sin\left(\frac{\theta}{2}\right) \cos\left(\frac{\theta}{2}\right) \cos\left(\frac{3\theta}{2}\right)$
τ_{xy}	$\frac{K_I}{\sqrt{2\pi r}} \cos\left(\frac{\theta}{2}\right) \sin\left(\frac{\theta}{2}\right) \cos\left(\frac{3\theta}{2}\right)$	$\frac{K_{II}}{\sqrt{2\pi r}} \cos\left(\frac{\theta}{2}\right) \left[1 - \sin\left(\frac{\theta}{2}\right) \sin\left(\frac{3\theta}{2}\right) \right]$
σ_{zz}	0 (Plane stress) $v(\sigma_{xx} + \sigma_{yy})$ (Plane strain)	0 (Plane stress) $v(\sigma_{xx} + \sigma_{yy})$ (Plane strain)
τ_{xz}, τ_{yz}	0	0

Note: v is Poisson's ratio.

material can be written as

$$\lim_{r \rightarrow 0} \sigma_{ij}^{(I)} = \frac{K_I}{\sqrt{2\pi r}} f_{ij}^{(I)}(\theta) \quad (2.37a)$$

$$\lim_{r \rightarrow 0} \sigma_{ij}^{(II)} = \frac{K_{II}}{\sqrt{2\pi r}} f_{ij}^{(II)}(\theta) \quad (2.37b)$$

$$\lim_{r \rightarrow 0} \sigma_{ij}^{(III)} = \frac{K_{III}}{\sqrt{2\pi r}} f_{ij}^{(III)}(\theta) \quad (2.37c)$$

for Modes I, II, and III, respectively. In a mixed-mode problem (i.e., when more than one loading mode is present), the individual contributions to a given stress component are additive:

$$\sigma_{ij}^{(\text{total})} = \sigma_{ij}^{(I)} + \sigma_{ij}^{(II)} + \sigma_{ij}^{(III)} \quad (2.38)$$

Equation (2.38) stems from the principle of linear superposition.

Detailed expressions for the singular stress fields for Mode I and Mode II are given in Table 2.1. Displacement relationships for Mode I and Mode II are listed in Table 2.2. Table 2.3 lists the nonzero stress and displacement components for Mode III.

TABLE 2.2
Crack-Tip Displacement Fields for Mode I and Mode II
(Linear Elastic, Isotropic Material)

	Mode I	Mode II
u_x	$\frac{K_I}{2\mu} \sqrt{\frac{r}{2\pi}} \cos\left(\frac{\theta}{2}\right) \left[\kappa - 1 + 2\sin^2\left(\frac{\theta}{2}\right) \right]$	$\frac{K_{II}}{2\mu} \sqrt{\frac{r}{2\pi}} \sin\left(\frac{\theta}{2}\right) \left[\kappa + 1 + 2\cos^2\left(\frac{\theta}{2}\right) \right]$
u_y	$\frac{K_I}{2\mu} \sqrt{\frac{r}{2\pi}} \sin\left(\frac{\theta}{2}\right) \left[\kappa + 1 - 2\cos^2\left(\frac{\theta}{2}\right) \right]$	$-\frac{K_{II}}{2\mu} \sqrt{\frac{r}{2\pi}} \cos\left(\frac{\theta}{2}\right) \left[\kappa - 1 - 2\sin^2\left(\frac{\theta}{2}\right) \right]$

Note: μ is the shear modulus. $\kappa = 3 - 4v$ (plane strain) and $\kappa = (3 - v)/(1 + v)$ (plane stress).

TABLE 2.3
Nonzero Stress and Displacement Components in Mode III
(Linear Elastic, Isotropic Material)

$$\tau_{xz} = -\frac{K_{III}}{\sqrt{2\pi r}} \sin\left(\frac{\theta}{2}\right)$$

$$\tau_{yz} = \frac{K_{III}}{\sqrt{2\pi r}} \cos\left(\frac{\theta}{2}\right)$$

$$u_z = \frac{2K_{III}}{\mu} \sqrt{\frac{r}{2\pi}} \sin\left(\frac{\theta}{2}\right)$$

Consider the Mode I singular field on the crack plane, where $\theta = 0$. According to Table 2.1, the stresses in the x and y direction are equal:

$$\sigma_{xx} = \sigma_{yy} = \frac{K_I}{\sqrt{2\pi r}} \quad (2.39)$$

When $\theta = 0$, the shear stress is zero, which means that the crack plane is a principal plane for pure Mode I loading. Figure 2.15 is a schematic plot of σ_{yy} , the stress normal to the crack plane vs. distance from the crack tip. Equation (2.39) is valid only near the crack tip, where the $1/\sqrt{r}$ singularity dominates the stress field. Stresses far from the crack tip are governed by the remote boundary conditions. For example, if the cracked structure is subjected to a uniform remote tensile stress, σ_{yy} approaches a constant value σ^∞ . We can define a *singularity-dominated zone* as the region where the equations in Table 2.1 to Table 2.3 describe the crack-tip fields.

The stress intensity factor defines the amplitude of the crack-tip singularity. That is, stresses near the crack tip increase in proportion to K . Moreover, the stress intensity factor completely defines the crack tip conditions; if K is known, it is possible to solve for all components of stress, strain, and displacement as a function of r and θ . This single-parameter description of crack tip conditions turns out to be one of the most important concepts in fracture mechanics.

2.6.2 RELATIONSHIP BETWEEN K AND GLOBAL BEHAVIOR

In order for the stress intensity factor to be useful, one must be able to determine K from remote loads and the geometry. Closed-form solutions for K have been derived for a number of simple

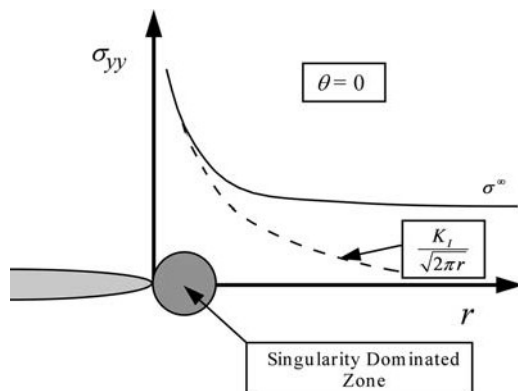


FIGURE 2.15 Stress normal to the crack plane in Mode I.

configurations. For more complex situations, the stress intensity factor can be estimated by experiment or numerical analysis (see Chapter 12).

One configuration for which a closed-form solution exists is a through crack in an infinite plate subjected to a remote tensile stress (Figure 2.3). Since the remote stress σ is perpendicular to the crack plane, the loading is pure Mode I. Linear elastic bodies must undergo proportional stressing, i.e., all the stress components at all locations increase in proportion to the remotely applied forces. Thus the crack-tip stresses must be proportional to the remote stress, and $K_I \propto \sigma$. According to Equation (2.37), stress intensity has units of stress $\bullet \sqrt{\text{length}}$. Since the only relevant length scale in Figure 2.3 is the crack size, the relationship between K_I and the global conditions must have the following form:

$$K_I = O(\sigma \sqrt{a}) \quad (2.40)$$

The actual solution, which is derived in Appendix 2.3, is given by

$$K_I = \sigma \sqrt{\pi a} \quad (2.41)$$

Thus the amplitude of the crack-tip singularity for this configuration is proportional to the remote stress and the square root of the crack size. The stress intensity factor for Mode II loading of the plate in Figure 2.3 can be obtained by replacing σ in Equation (2.41) by the remotely applied shear stress (see Figure 2.18 and Equation (2.43) below).

A related solution is that for a semi-infinite plate with an edge crack (Figure 2.16). Note that this configuration can be obtained by slicing the plate in Figure 2.3 through the middle of the crack. The stress intensity factor for the edge crack is given by

$$K_I = 1.12\sigma \sqrt{\pi a} \quad (2.42)$$

which is similar to Equation (2.41). The 12% increase in K_I for the edge crack is caused by different boundary conditions at the free edge. As Figure 2.17 illustrates, the edge crack opens more because it is less restrained than the through crack, which forms an elliptical shape when loaded.

Consider a through crack in an infinite plate where the normal to the crack plane is oriented at an angle β with the stress axis (Figure 2.18(a)). If $\beta \neq 0$, the crack experiences combined Mode I and Mode II loading; $K_{II} = 0$ as long as the stress axis and the crack normal both lie in the plane of the plate. If we redefine the coordinate axis to coincide with the crack orientation (Figure 2.18(b)), we see that the applied stress can be resolved into normal and shear components. The stress normal to the crack plane, $\sigma_{yy'}$, produces pure Mode I loading, while $\tau_{xy'}$ applies Mode II loading to the crack. The stress intensity factors for the plate in Figure 2.18 can be inferred by relating $\sigma_{yy'}$ and $\tau_{xy'}$ to σ and β through Mohr's circle:

$$\begin{aligned} K_I &= \sigma_{yy'} \sqrt{\pi a} \\ &= \sigma \cos^2(\beta) \sqrt{\pi a} \end{aligned} \quad (2.43a)$$

and

$$\begin{aligned} K_{II} &= \tau_{xy'} \sqrt{\pi a} \\ &= \sigma \sin(\beta) \cos(\beta) \sqrt{\pi a} \end{aligned} \quad (2.43b)$$

Note that Equation (2.43) reduces to the pure Mode I solution when $\beta = 0$. The maximum K_{II} occurs at $\beta = 45^\circ$, where the shear stress is also at a maximum. Section 2.11 addresses fracture under mixed mode conditions.

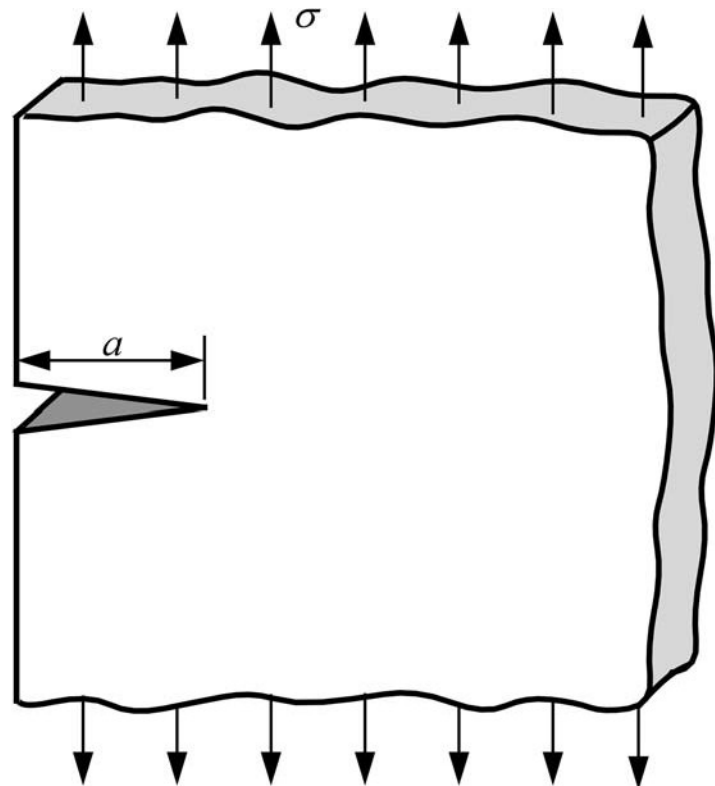


FIGURE 2.16 Edge crack in a semi-infinite plate subject to a remote tensile stress.

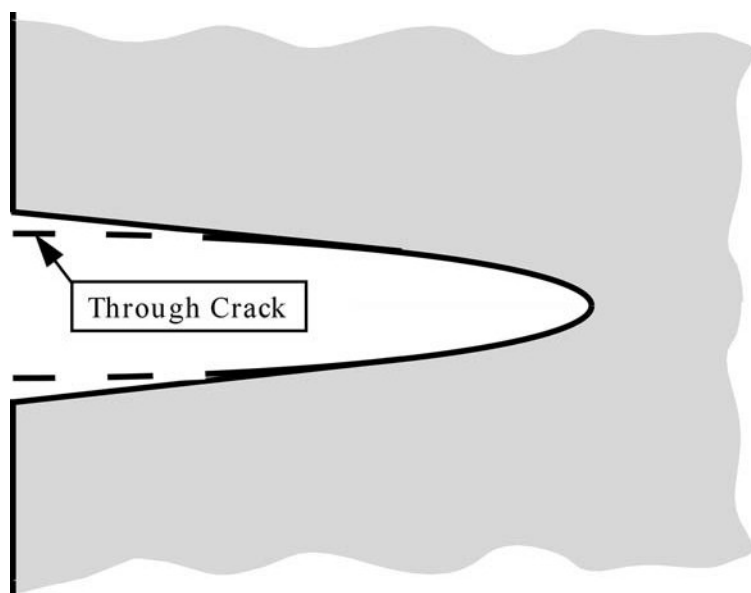


FIGURE 2.17 Comparison of crack-opening displacements for an edge crack and through crack. The edge crack opens wider at a given stress, resulting in a stress intensity that is 12% higher.

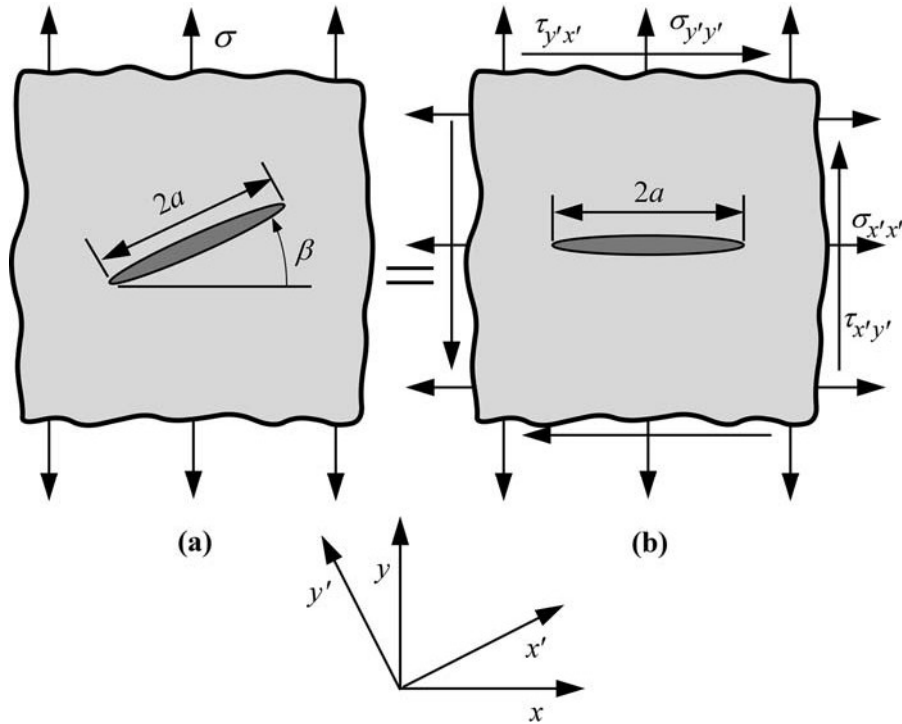


FIGURE 2.18 Through crack in an infinite plate for the general case where the principal stress is not perpendicular to the crack plane.

The penny-shaped crack in an infinite medium (Figure 2.4) is another configuration for which a closed-form K_I solution exists [11]:

$$K_I = \frac{2}{\pi} \sigma \sqrt{\pi a} \quad (2.44)$$

where a is the crack radius. Note that Equation (2.44) has the same form as the previous relationships for a through crack, except that the crack radius is the characteristic length in the above equation. The more general case of an elliptical or semielliptical flaw is illustrated in Figure 2.19. In this instance, two length dimensions are needed to characterize the crack size: $2c$ and $2a$, the major and minor axes of the ellipse, respectively (see Figure 2.19). Also, when $a < c$, the stress intensity factor varies along the crack front, with the maximum K_I at $\phi = 90^\circ$. The flaw shape parameter Q is obtained from an elliptic integral, as discussed in Appendix 2.4. Figure 2.19 gives an approximate solution for Q . The surface correction factor λ_s is also an approximation.

2.6.3 EFFECT OF FINITE SIZE

Most configurations for which there is a closed-form K solution consist of a crack with a simple shape (e.g., a rectangle or ellipse) in an infinite plate. Stated another way, the crack dimensions are small compared to the size of the plate; the crack-tip conditions are not influenced by external boundaries. As the crack size increases, or as the plate dimensions decrease, the outer boundaries begin to exert an influence on the crack tip. In such cases, a closed-form stress intensity solution is usually not possible.

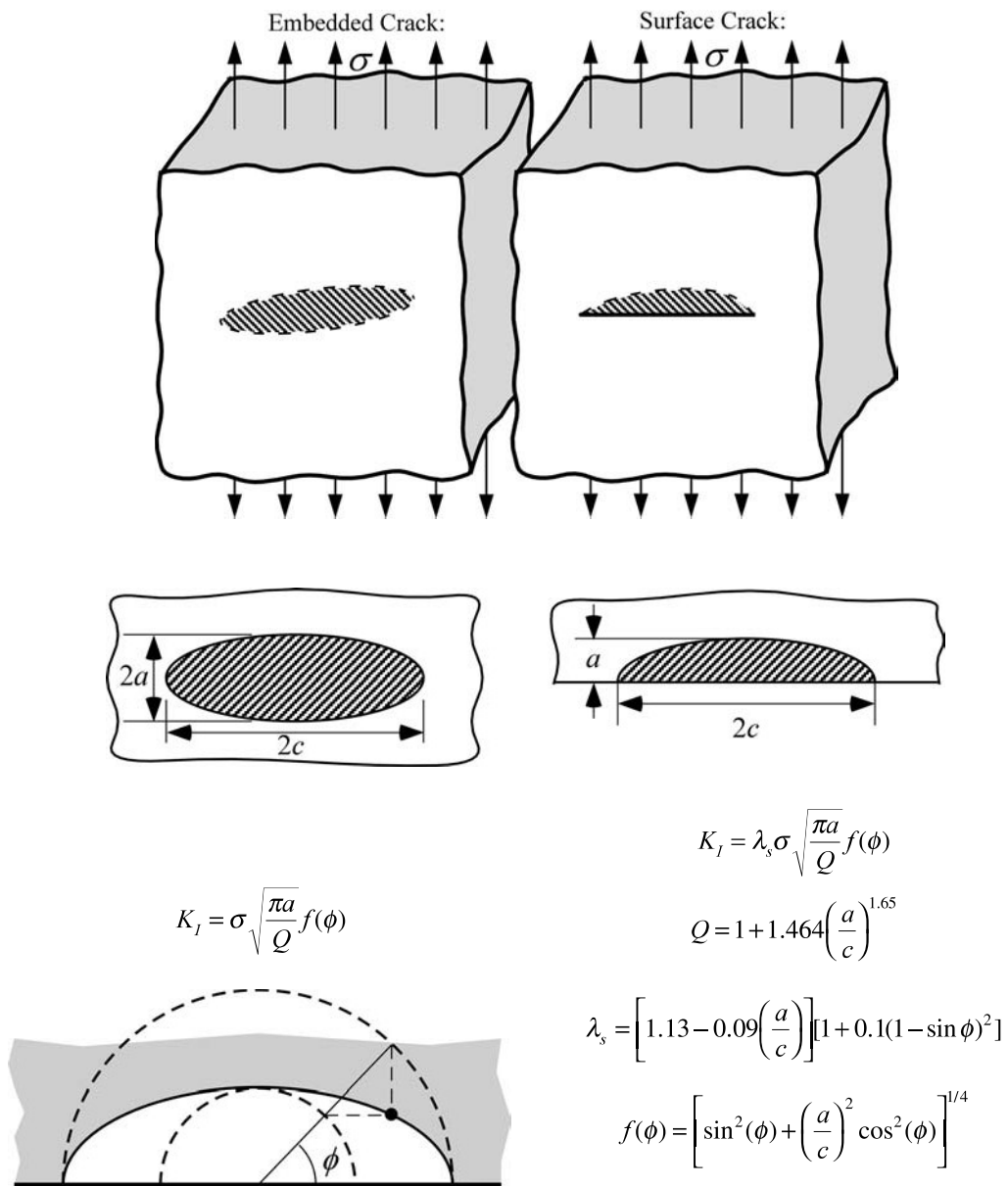


FIGURE 2.19 Mode I stress intensity factors for elliptical and semielliptical cracks. These solutions are valid only as long as the crack is small compared to the plate dimensions and $a \leq c$.

Consider a cracked plate subjected to a remote tensile stress. Figure 2.20 schematically illustrates the effect of finite width on the crack tip stress distribution, which is represented by lines of force; the local stress is proportional to the spacing between lines of force. Since a tensile stress cannot be transmitted through a crack, the lines of force are diverted around the crack, resulting in a local stress concentration. In the infinite plate, the line of force at a distance W from the crack centerline has force components in the x and y directions. If the plate width is restricted to $2W$, the x force must be zero on the free edge; this boundary condition causes the lines of force to be compressed, which results in a higher stress intensification at the crack tip.

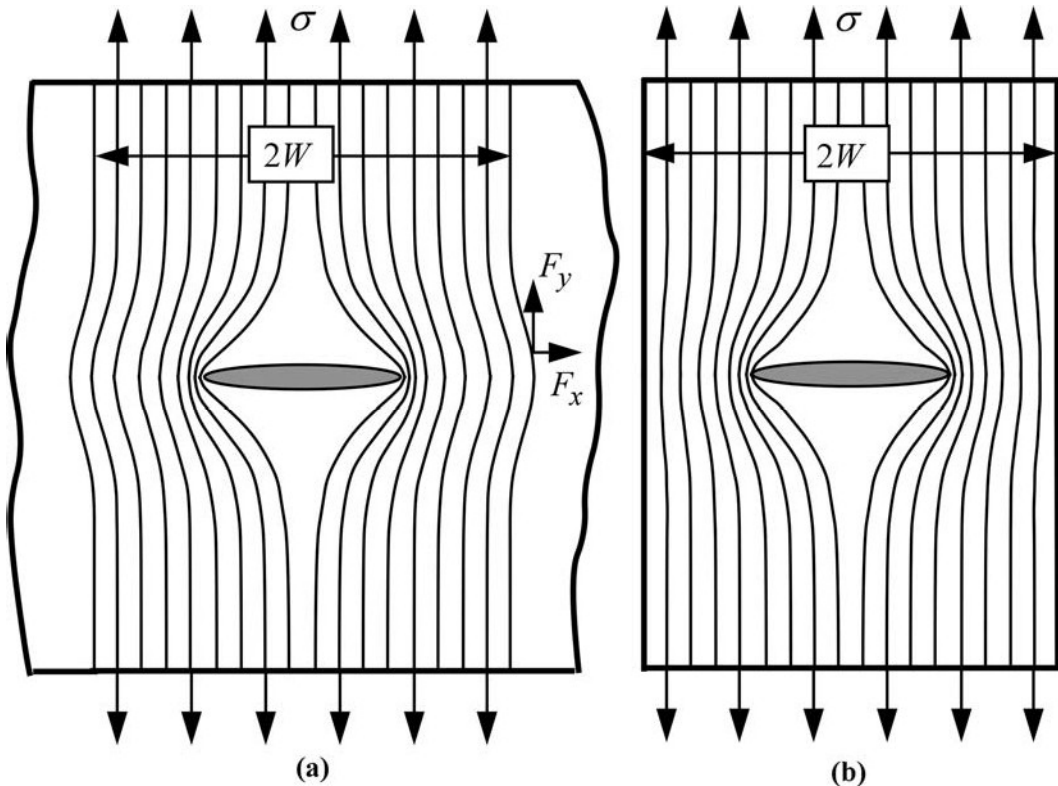


FIGURE 2.20 Stress concentration effects due to a through crack in finite and infinite width plates: (a) infinite plate and (b) finite plate.

One technique to approximate the finite width boundary condition is to assume a periodic array of collinear cracks in an infinite plate (Figure 2.21). The Mode I stress intensity factor for this situation is given by

$$K_I = \sigma \sqrt{\pi a} \left[\frac{2W}{\pi a} \tan\left(\frac{\pi a}{2W}\right) \right]^{1/2} \quad (2.45)$$

The stress intensity approaches the infinite plate value as a/W approaches zero; K_I is asymptotic to $a/W = 1$.

More accurate solutions for a through crack in a finite plate have been obtained from finite-element analysis; solutions of this type are usually fit to a polynomial expression. One such solution [12] is given by

$$K_I = \sigma \sqrt{\pi a} \left[\sec\left(\frac{\pi a}{2W}\right)^{1/2} \right] \left[1 - 0.025 \left(\frac{a}{W} \right)^2 + 0.06 \left(\frac{a}{W} \right)^4 \right] \quad (2.46)$$

Figure 2.22 compares the finite width corrections in Equation (2.45) and Equation (2.46). The secant term (without the polynomial term) in Equation (2.46) is also plotted. Equation (2.45) agrees with the finite-element solution to within 7% for $a/W < 0.6$. The secant correction is much closer to the finite element solution; the error is less than 2% for $a/W < 0.9$. Thus, the polynomial term in Equation (2.46) contributes little and can be neglected in most cases.

Table 2.4 lists stress intensity solutions for several common configurations. These K_I solutions are plotted in Figure 2.23. Several handbooks devoted solely to stress intensity solutions have been published [12–14].

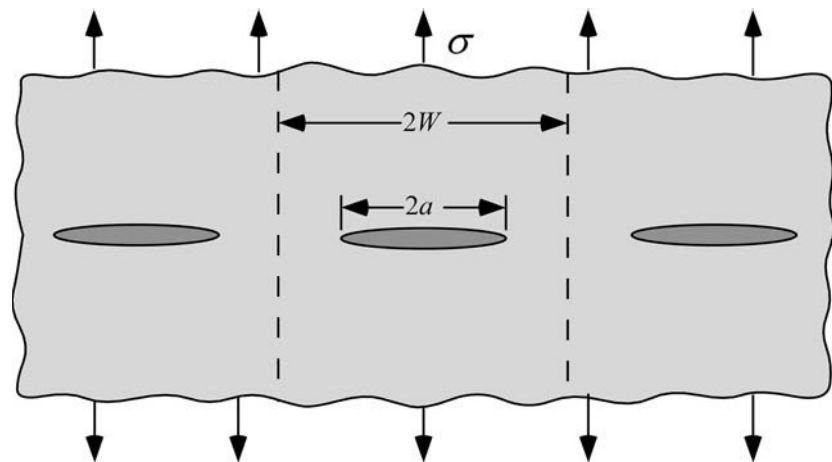


FIGURE 2.21 Collinear cracks in an infinite plate subject to remote tension.

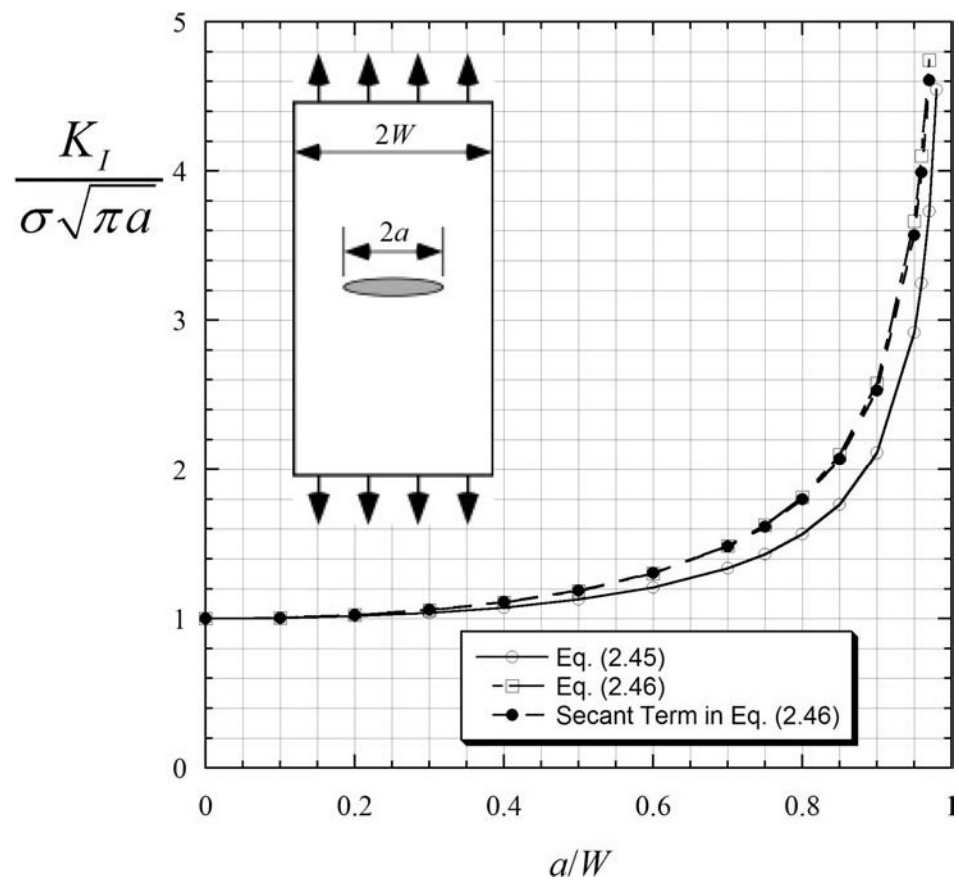
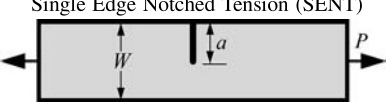
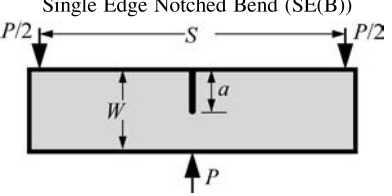
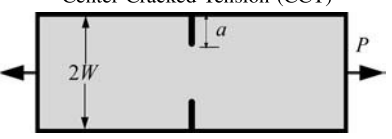
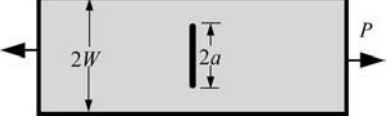
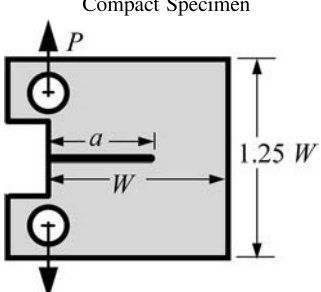


FIGURE 2.22 Comparison of finite width corrections for a center-cracked plate in tension.

TABLE 2.4
 K_I Solutions for Common Test Specimens^a

GEOMETRY	$f\left(\frac{a}{W}\right)^*$
Single Edge Notched Tension (SENT) 	$\begin{aligned} & f\left(\frac{a}{W}\right)^* \\ & \frac{\sqrt{2\tan\frac{\pi a}{2W}}}{\cos\frac{\pi a}{2W}} \left[0.752 + 2.02\left(\frac{a}{W}\right) \right] \\ & + 0.37\left(1 - \sin\frac{\pi a}{2W}\right)^3 \end{aligned}$
Single Edge Notched Bend (SE(B)) 	$\begin{aligned} & \frac{3S}{W} \sqrt{\frac{a}{W}} \\ & \frac{2\left(1+2\frac{a}{W}\right)\left(1-\frac{a}{W}\right)^{3/2}}{\left(1-\frac{a}{W}\right)} \left[1.99 - \frac{a}{W} \right. \\ & \left. \left(1-\frac{a}{W}\right) \left\{ 2.15 - 3.93\left(\frac{a}{W}\right) + 2.7\left(\frac{a}{W}\right)^2 \right\} \right] \end{aligned}$
Center Cracked Tension (CCT) 	$\begin{aligned} & \sqrt{\frac{\pi a}{4W}} \sec\left(\frac{\pi a}{2W}\right) \left[1 - 0.025\left(\frac{a}{W}\right)^2 \right. \\ & \left. + 0.06\left(\frac{a}{W}\right)^4 \right] \end{aligned}$
Double Edge Notched Tension (DENT) 	$\begin{aligned} & \frac{\sqrt{\frac{\pi a}{2W}}}{\sqrt{1-\frac{a}{W}}} \left[1.122 - 0.561\left(\frac{a}{W}\right) - 0.205\left(\frac{a}{W}\right)^2 \right. \\ & \left. + 0.471\left(\frac{a}{W}\right)^3 + 0.190\left(\frac{a}{W}\right)^4 \right] \end{aligned}$
Compact Specimen 	$\begin{aligned} & \frac{2+\frac{a}{W}}{\left(1-\frac{a}{W}\right)^{3/2}} \left[0.886 + 4.64\left(\frac{a}{W}\right) - 13.32\left(\frac{a}{W}\right)^2 \right. \\ & \left. + 14.72\left(\frac{a}{W}\right)^3 - 5.60\left(\frac{a}{W}\right)^4 \right] \end{aligned}$

$$*K_I = \frac{P}{B\sqrt{W}} f\left(\frac{a}{W}\right) \quad \text{where } B \text{ is the specimen thickness.}$$

^a Taken from Tada, H., Paris, P.C., and Irwin, G.R., *The Stress Analysis of Cracks Handbook*, 2nd Ed., Paris Productions, St. Louis, MO, 1985.

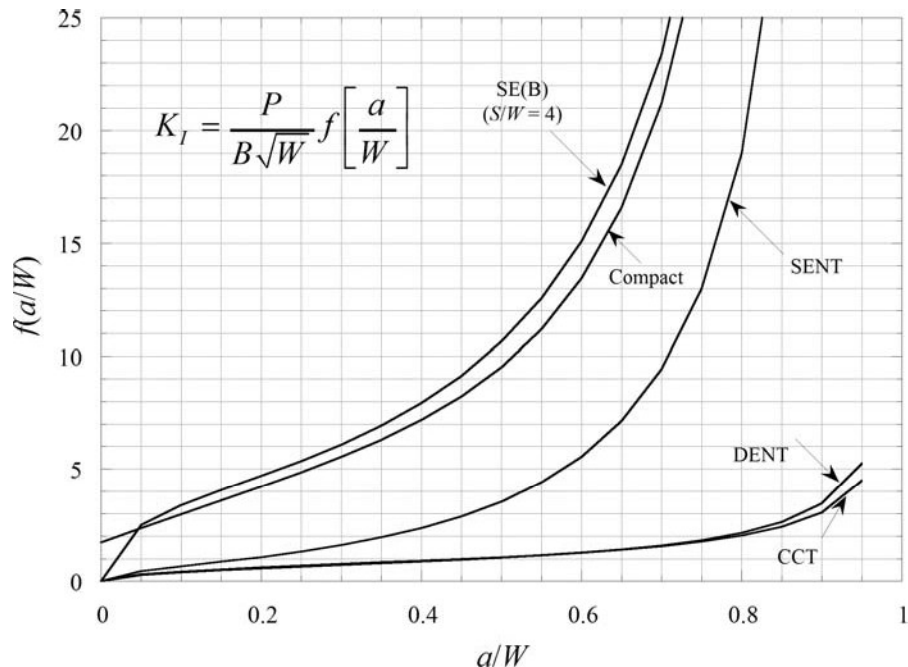


FIGURE 2.23 Plot of stress intensity solutions from Table 2.4.

Although stress intensity solutions are given in a variety of forms, K can always be related to the through crack (Figure 2.4) through the appropriate correction factor:

$$K_{(I,II,III)} = Y\sigma\sqrt{\pi a} \quad (2.47)$$

where

σ = characteristic stress

a = characteristic crack dimension

Y = dimensionless constant that depends on the geometry and the mode of loading

EXAMPLE 2.4

Show that the K_I solution for the single edge notched tensile panel reduces to Equation (2.42) when $a \ll W$.

Solution: All of the K_I expressions in Table 2.4 are of the form:

$$K_I = \frac{P}{B\sqrt{W}} f\left(\frac{a}{w}\right)$$

where

P = applied force

B = plate thickness

$f(a/w)$ = dimensionless function

The above equation can be expressed in the form of Equation (2.47):

$$\frac{P}{B\sqrt{W}} f\left(\frac{a}{w}\right) = \frac{P}{BW} f\left(\frac{a}{w}\right) \sqrt{\frac{W}{\pi a}} = Y\sigma \sqrt{\pi a}$$

where

$$Y = f\left(\frac{a}{W}\right) \sqrt{\frac{W}{\pi a}}$$

In the limit of a small flaw, the geometry correction factor in Table 2.4 becomes

$$\lim_{a/W \rightarrow 0} f\left(\frac{a}{W}\right) = \sqrt{\frac{\pi a}{W}} (0.752 + 0.37)$$

Thus,

$$\lim_{a/W \rightarrow 0} f(Y) = 1.12$$

2.6.4 PRINCIPLE OF SUPERPOSITION

For linear elastic materials, individual components of stress, strain, and displacement are additive. For example, two normal stresses in the x direction imposed by different external forces can be added to obtain the total σ_{xx} , but a normal stress cannot be summed with a shear stress. Similarly, stress intensity factors are additive as long as the mode of loading is consistent. That is

$$K_I^{(\text{total})} = K_I^{(A)} + K_I^{(B)} + K_I^{(C)}$$

but

$$K_{(\text{total})} \neq K_I + K_{II} + K_{III}$$

In many instances, the principle of superposition allows stress intensity solutions for complex configurations to be built from simple cases for which the solutions are well established. Consider, for example, an edge-cracked panel (Table 2.4) subject to combined membrane (axial) loading P_m , and three-point bending P_b . Since both types of loading impose pure Mode I conditions, the K_I values can be added:

$$\begin{aligned} K_I^{(\text{total})} &= K_I^{(\text{membrane})} + K_I^{(\text{bending})} \\ &= \frac{1}{B\sqrt{W}} \left[P_m f_m \left(\frac{a}{W} \right) + P_b f_b \left(\frac{a}{W} \right) \right] \end{aligned} \quad (2.48)$$

where f_m and f_b are the geometry correction factors for membrane and bending loading, respectively, listed in Table 2.4 and plotted in Figure 2.23.

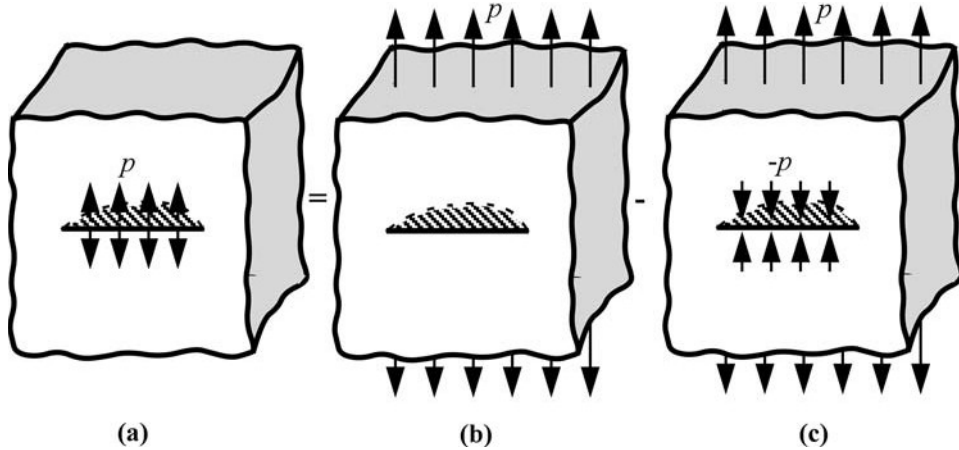


FIGURE 2.24 Determination of K_I for a semielliptical surface crack under internal pressure p by means of the principle of superposition.

EXAMPLE 2.5

Determine the stress intensity factor for a semielliptical surface crack subjected to an internal pressure p (Figure 2.24(a)).

Solution: The principle of superposition enables us to construct the solution from known cases. One relevant case is the semielliptical surface flaw under uniform remote tension p (Figure 2.24(b)). If we impose a uniform compressive stress $-p$ on the crack surface (Figure 2.24(c)), $K_I = 0$ because the crack faces close, and the plate behaves as if the crack were not present. The loading configuration of interest is obtained by subtracting the stresses in Figure 2.24(c) from those of Figure 2.24(b):

$$\begin{aligned} K_I^{(a)} &= K_I^{(b)} - K_I^{(c)} \\ &= \lambda_s p \sqrt{\frac{\pi a}{Q}} f(\phi) - 0 = \lambda_s p \sqrt{\frac{\pi a}{Q}} f(\phi) \end{aligned}$$

Example 2.5 is a simple illustration of a more general concept, namely, stresses acting on the boundary (i.e., tractions) can be replaced with tractions that act on the crack face, such that the two loading configurations (boundary tractions vs. crack-face tractions) result in the same stress intensity factor. Consider an uncracked body subject to a boundary traction $P(x)$, as illustrated in Figure 2.25. This boundary traction results in a normal stress distribution $p(x)$ on Plane A-B. In order to confine the problem to Mode I, let us assume that no shear stresses act on Plane A-B. (This assumption is made only for the sake of simplicity; the basic principle can be applied to all three modes of loading.) Now assume that a crack that forms on Plane A-B and the boundary traction $P(x)$ remains fixed, as Figure 2.26(a) illustrates. If we remove the boundary traction and apply a traction $p(x)$ on the crack face (Figure 2.26(b)), the principle of superposition indicates that the applied K_I will be unchanged. That is

$$K_I^{(a)} = K_I^{(b)} - K_I^{(c)} = K_I^{(b)} \quad (\text{since } K_I^{(c)} = 0)$$

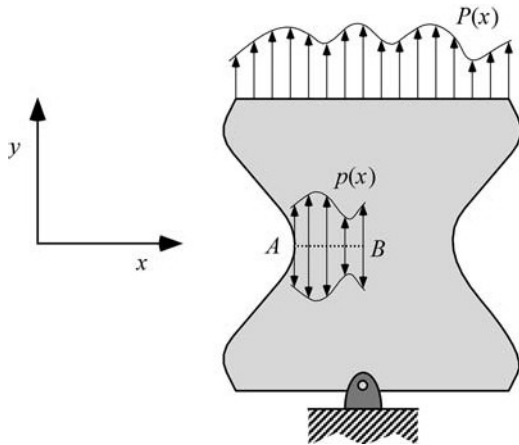


FIGURE 2.25 Uncracked body subject to an arbitrary boundary traction $P(x)$, which results in a normal stress distribution $p(x)$ acting on Plane A-B.

2.6.5 WEIGHT FUNCTIONS

When one performs an analysis to infer a stress intensity factor for a cracked body, the K value that is computed applies only to one particular set of boundary conditions; different loading conditions result in a different stress intensity factors for that geometry. It turns out, however, that the solution to one set of boundary conditions contains sufficient information to infer K for *any other* boundary conditions on that same geometry.

Consider two arbitrary loading conditions on an isotropic elastic cracked body in plane stress or plane strain. For now, we assume that both loadings are symmetric with respect to the crack plane, such that pure Mode I loading is achieved in each case. Suppose that we know the stress intensity factor for loading (1) and we wish to solve for $K_I^{(2)}$, the stress intensity factor for the second set of boundary conditions. Rice [15] showed that $K_I^{(1)}$ and $K_I^{(2)}$ are related as follows:

$$K_I^{(2)} = \frac{E'}{2K_I^{(1)}} \left[\int_{\Gamma} T_i \frac{\partial u_i^{(1)}}{\partial a} d\Gamma + \int_A F_i \frac{\partial u_i^{(1)}}{\partial a} dA \right] \quad (2.49)$$

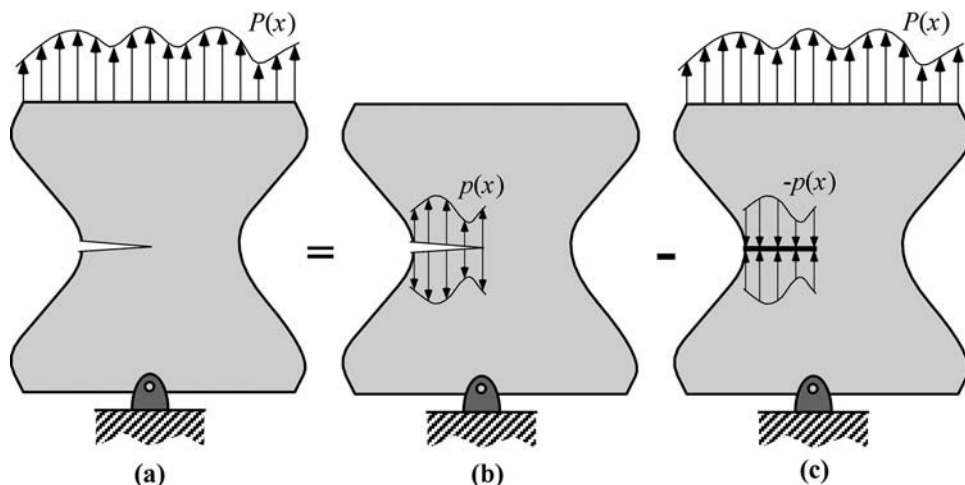


FIGURE 2.26 Application of superposition to replace a boundary traction $P(x)$ with a crack face traction $p(x)$ that results in the same K_I .

where Γ and A are the perimeter and area of the body, respectively, and u_i are the displacements in the x and y directions. Since loading systems (1) and (2) are arbitrary, it follows that $K_I^{(2)}$ cannot depend on $K_I^{(1)}$ and $u_i^{(1)}$. Therefore, the function

$$h(x_i) = \frac{E}{2K_I^{(1)}} \frac{\partial u_i^{(1)}}{\partial a} \quad (2.50)$$

where x_i represents the x and y coordinates, must be independent of the nature of loading system (1). Bueckner [16] derived a similar result to Equation (2.50) two years before Rice, and referred to h as a *weight function*.

Weight functions are first-order tensors that depend only on the geometry of the cracked body. Given the weight function for a particular configuration, it is possible to compute K_I from Equation (2.49) for any boundary condition. Moreover, the previous section invoked the principle of superposition to show that any loading configuration can be represented by appropriate tractions applied directly to the crack face. Thus K_I for a two-dimensional cracked body can be inferred from the following expression:

$$K_I = \int_{\Gamma_c} p(x)h(x)dx \quad (2.51)$$

where $p(x)$ is the crack face traction (equal to the normal stress acting on the crack plane when the body is uncracked) and Γ_c is the perimeter of the crack. The weight function $h(x)$ can be interpreted as the stress intensity resulting from a unit force applied to the crack face at x , and the above integral represents the superposition of the K_I values from discrete opening forces along the crack face.

EXAMPLE 2.6

Derive an expression for K_I for an arbitrary traction on the face of a through crack in an infinite plate.

Solution: We already know K_I for this configuration when a uniform tensile stress is applied:

$$K_I = \sigma \sqrt{\pi a}$$

where a is the half-crack length. From Equation (A2.43), the opening displacement of the crack faces in this case is given by

$$u_y = \pm \frac{2\sigma}{E'} \sqrt{x(2a-x)}$$

where the x - y coordinate axis is defined in Figure 2.27(a). Since the crack length is $2a$, we must differentiate u_y with respect to $2a$ rather than a :

$$\frac{\partial u_y}{\partial(2a)} = \pm \frac{2\sigma}{E} \sqrt{\frac{x}{2a-x}}$$

Thus, the weight function for this crack geometry is given by

$$h(x) = \pm \frac{1}{\sqrt{\pi a}} \sqrt{\frac{x}{2a-x}}$$

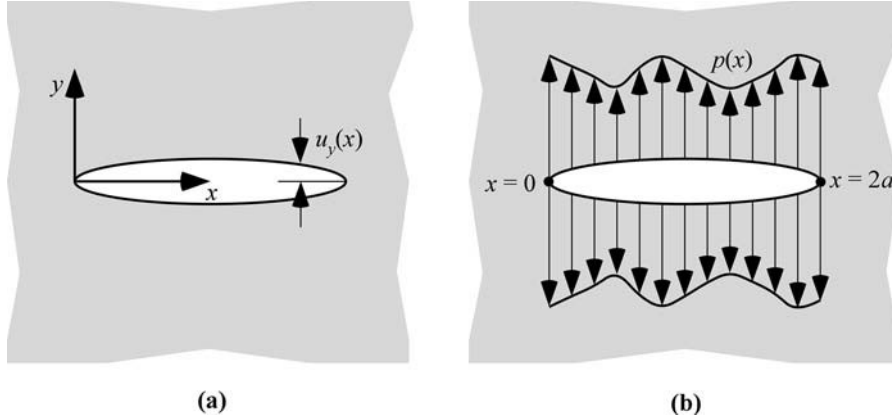


FIGURE 2.27 Through crack configuration analyzed in Example 2.6: (a) definition of coordinate axes and (b) arbitrary traction applied to crack faces.

If we apply a surface traction of $\pm p(x)$ on the crack faces, the Mode I stress intensity factor for the two crack tips is as follows:

$$K_{I(x=2a)} = \frac{1}{\sqrt{\pi a}} \int_0^{2a} p(x) \sqrt{\frac{x}{2a-x}} dx$$

$$K_{I(x=0)} = \frac{1}{\sqrt{\pi a}} \int_0^{2a} p(x) \sqrt{\frac{2a-x}{x}} dx$$

The weight function concept is not restricted to two-dimensional bodies, Mode I loading, or isotropic elastic materials. In their early work on weight functions, Rice [15] extended the theory to three dimensions, Bueckner [16] considered combined Mode I/II loading, and both allowed for anisotropy in the elastic properties. Subsequent researchers [17–22] have shown that the theory applies to all linear elastic bodies that contain an arbitrary number of cracks.

For mixed-mode problems, separate weight functions are required for each mode: h_I , h_{II} , and h_{III} . Since the stress intensity factors can vary along a three-dimensional crack front, the weight functions also vary along the crack front. That is

$$h_\alpha = h_\alpha(x_i, \eta) \quad (2.52)$$

where $\alpha (= 1, 2, 3)$ indicates the mode of loading and η is the crack front position.

Given that any loading configuration in a cracked body can be represented by equivalent crack-face tractions, the general mixed-mode, three-dimensional formulation of the weight function approach can be expressed in the following form:

$$K_\alpha(\eta) = \int_{S_c} T_i h_\alpha(x_i, \eta) dS \quad (2.53)$$

where T_i are the tractions assumed to act on the crack surface S_c .

See Chapter 9 for examples of practical applications of weight functions.

2.7 RELATIONSHIP BETWEEN K AND G

Two parameters that describe the behavior of cracks have been introduced so far: the energy release rate and the stress intensity factor. The former parameter quantifies the net change in potential